Heat-Driven Acoustic Phonons in Lamellar Nanoplatelet Assemblies

Journal:	*Nanoscale*
Manuscript ID	NR-ART-01-2020-000695.R2
Article Type:	Paper
Date Submitted by the Author:	10-Apr-2020
Complete List of Authors:	Diroll, Benjamin; Argonne National Laboratory, Center for Nanoscale Materials Kamysbayev, Vlad; University of Chicago Division of the Physical Sciences, Chemistry Coropceanu, Igor; University of Chicago Division of the Physical Sciences, Chemistry Talapin, Dmitri; The University of Chicago, Department of Chemistry Schaller, Richard; Argonne National Laboratory, Center for Nanoscale Materials

SCHOLARONE™
Manuscripts

Heat-Driven Acoustic Phonons in Lamellar Nanoplatelet Assemblies

Received 00th January 20xx,
Accepted 00th January 20xx

DOI: 10.1039/x0xx00000x

Benjamin T. Diroll,[a*] Vladislav Kamysbayev,[b] Igor Coropceanu,[b] and Dmitri V. Talapin.[a,b] Richard D. Schaller[a,c]

Colloidal CdSe nanoplatelets, with the electronic structure of quantum wells, self-assemble into lamellar stacks due to large co-facial van der Waals attractions. These lamellar stacks are shown to display coherent acoustic phonons that are detected from oscillatory changes in the absorption spectrum observed in infrared pump, electronic probe measurements. Rather than direct electronic excitation of the nanocrystals using a femtosecond laser, impulsive transfer of heat from the organic ligand shell, excited at C-H stretching vibrational resonances, to the inorganic core of individual nanoplatelets occurs on a time-scale of < 100 ps. This heat transfer is drives in-phase longitudinal acoustic phonons of the nanoplatelet lamellae, which are accompanied by subtle deformations along the nanoplatelet short axes. The frequencies of the oscillations vary from 0.7 to 2 GHz (3-8 μeV and 0.5-1 ns oscillation period) depending on the thickness of the nanoplatelets—but not their lateral areas—and the temperature of the sample. Temperature-dependence of the acoustic phonon frequency conveys a substantial stiffening of the organic ligand “bonds” between nanoplatelets with reduced temperature. These results demonstrate a potential for acoustic modulation of the excitonic structure of nanocrystal assemblies in self-assembled anisotropic semiconductor systems at temperatures at or above 300 K.

Introduction

Semiconductor nanocrystal solids offer promise for a host of solid-state optoelectronic technologies including solar cells,[1] photodetectors,[2] thermoelectric devices,[3] transistors,[4] lasers,[5] and light-emitting diodes.[6] Chiefly, these applications are supposed to benefit from the unique electronic structure conferred by quantum confinement[7,8] but important properties of nanocrystal solids like thermal conductivity are governed by phonons and interfacial properties in those materials.[9,10] Although most nanocrystal-based materials have only local interparticle ordering, nanocrystal superlattices[11] with long-range ordering show richer phonon structure[10,12] and provide a framework for mechanical behavior in other nanocrystal solids.[13,14] Limited studies of phonons in extended nanocrystal arrays employ high-resolution Raman spectroscopy[15] or ultrafast optically-induced strain pulses.[12–14,16] Acoustic phonons induce periodic perturbations of the nanocrystal lattice which exploit deformation potentials to produce dynamic changes of absorption and reflectivity.[16] Examined predominantly in isolated metallic and semiconducting nanostructures,[17–33] coherent acoustic phonons have also been found in superlattices of nanoparticles.[12–14]

This work presents findings on acoustic phonons in colloidal cadmium selenide nanoplatelet (NPL) solids, evidenced from oscillatory changes of the NPL band gap. Unlike previous works, the self-assembled films are composed of highly anisotropic materials and the excitation source for the coherent acoustic phonons is a heat transfer process from the organic ligand shell of the NPLs to the inorganic cores rather than direct electronic excitation. Ordinarily, to generate a coherent acoustic phonon, excitations must be impulsive (much faster than the phonon period), and naturally most demonstrations of this phenomenon in individual nanocrystals and ensembles are performed using ultrafast (typically femtosecond) laser pulses. Here, because the observed phonon periods of spatially extended NPL stacks are hundreds of picoseconds, the transfer of heat on < 100 ps time-scale is functionally impulsive.

[a] Center for Nanoscale Materials, Argonne National Laboratory, Lemont, IL 60439, USA. E-mail: bdiroll@anl.gov
[b] Department of Chemistry, University of Chicago, Chicago, IL 60637, USA
[c] Department of Chemistry, Northwestern University, Evanston, IL 60208, USA

Electronic Supplementary Information (ESI) available: Additional experimental data and details included. See DOI: 10.1039/x0xx00000x

The highly-anisotropic NPLs used in this work form lamellar liquid-crystalline structures driven by strong co-facial van der Waals attractions.[34,35] The optically observed phonons exhibit exceptionally low frequencies (0.7 GHz to 2 GHz), which vary strongly with the thickness of the NPLs but are not sensitive to different lateral areas. Correlated with small-angle X-ray scattering (SAXS) data, these results implicate collective longitudinal acoustic phonons of the lamellar stacks as the origin of the oscillatory signal, rather than acoustic modes of individual NPLs. Longitudinal modes of the NPL stacks include concerted changes in the NPL short axes, which are exquisitely sensitive to changes in the thickness because of strong quantum confinement. A simple harmonic oscillator model, with "bonds" formed by surface-bound ligands between NPLs of defined mass is consistent with the observation of lower frequency oscillatory signals in thicker NPLs, although it underestimates the drop in frequency of phonons with increasing NPL thickness. With increasing temperature from 3 K to 350 K, the frequency of the observed acoustic phonon decreases by a factor of two, which provides evidence that the surface-bound organic ligands structurally disorder with elevated temperature, resulting in inter-NPL bonds of reduced strength, as consistent with studies of disorder in self-assembled monolayers.[36–39]

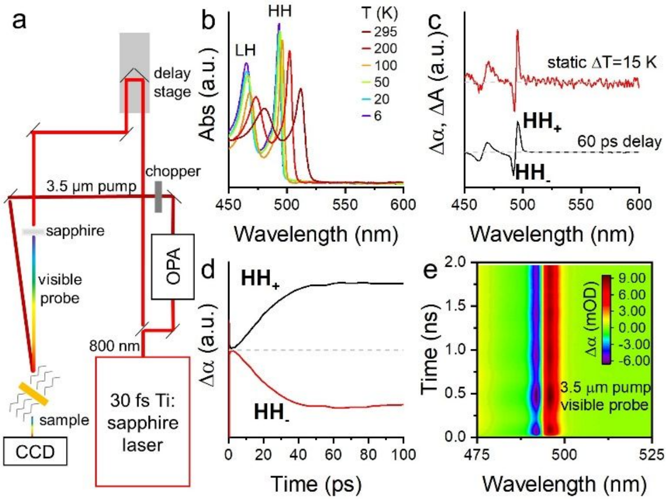

Figure 1. (a) Schematic of infrared pump, electronic probe (IPEP) experiment. (b) Static absorption spectra of a 4.5 ML CdSe nanoplatelet film at different temperatures with heavy- (HH) and light (LH) hole absorptions labelled. (c) Static differential absorption (ΔA) compared with transient differential absorption from IPEP experiment (Δα) at a delay time of 60 ps. The increased and decreased absorption at the heavy-hole feature (HH_+, HH_-) are indicated. The dashed gray line indicates no change in absorption. The static differential absorption spectra is referenced to the absorption at 6 K. (d) Line-cuts of the increased and decreased transient absorption features in IPEP experiments. The dashed gray line indicates no change in absorption. (e) Map of infrared pump, electronic probe (IPEP) transient absorption spectrum. The pump wavelength was centred around 3.5 µm and the probe was in the visible.

Results and Discussion

A Experimental Design

Figure 1a shows a schematic of the experimental design featured in this work. The NPLs, which comprise a mixture of myristic and oleic acid surface ligands on a CdSe inorganic NPL core,[40,41] display a strong mid-infrared absorption from the C-H vibrations of the ligands whereas the CdSe inorganic core is transparent in that spectral window. The high-energy vibrations of the organic ligand C-H stretches near 3500 nm can be used as antennae to couple heat into the NPLs with resonant infrared (IR) light excitation, which is manifest by a bathochromic shift of the CdSe band gap. In IR pump, electronic probe (IPEP) experiments,[41] a femtosecond pump laser is tuned to the infrared vibrational absorptions of the organic ligands (Supporting Information Figure S1) and subsequently probed at the band gap region of the NPLs to detect transient absorption changes (Δα) near the semiconductor band gap with heating. Pump excitation off-resonance with the vibrations of the ligands generates no signal other than a Stark effect.[41] These measurements trace the transfer of heat from the ligand to the inorganic core of the NPLs, as manifest by a red-shift of the optical absorption of the heated NPLs.

Figure 1b shows temperature-dependent static absorption spectra of a solid film of 4.5 monolayer (ML, here defined as a layer of cadmium and selenium atoms) CdSe NPLs. The NPL absorption blue-shifts and narrows at low temperature, although the integrated oscillator strength of the heavy hole (HH, first excitonic absorption) transition remains nearly constant.[42,43] As shown in Figure 1c, the difference spectrum of IPEP measurements (Δα) closely matches the difference spectrum (ΔA) induced by a temperature rise in static absorption spectra. By using the static differential absorption spectrum as a calibration,[41] the infrared pulses used in this work generate an estimated temperature rise of 15-20 K corresponding to a shift in the band gap (at 6 K) of < 500 µeV. Smaller temperature rises occur at higher temperatures where the specific heat capacity of the excited materials increases, but earlier measurements on quantum dots at cryogenic temperatures show comparable increases in temperature.[41,44] The sharp excitonic absorption lines enable the decreased absorption (HH_-) and increased absorption (HH_+) at the heavy hole absorption band arising from heating. The kinetic traces of the increased and decreased features in Figure 1d yield an empirical measurement of heat transfer from the vibrationally-excited organic ligands to the inorganic nanocrystal core. A flat slope of the Δα kinetic *versus* time (i.e. $\partial\Delta\alpha/\partial t = 0$) is evidence of no further temperature change of the CdSe core, indicative of a quasi-equilibrium. In this case, the signal rises over ~60 ps.

However, the band gap of the semiconductor NPLs continues to change over nanoseconds in an oscillatory manner with a period of hundreds of picoseconds as exemplified by the map of IPEP data in Figure 1e. Such oscillatory changes in absorption, which represent up to 30 % of the total Δα signal, are often signatures of acoustic phonons and similar behavior, albeit at higher frequencies, has been observed in many nanoscopic materials.[12–14,18,20,22,23,45] Unlike previous works, the excitation of the apparent acoustic phonon is due to the transfer of heat from the ligands to the inorganic core, not the laser pulse directly. Typically, to observe a coherent acoustic phonon, the excitation must be much faster than the period of the oscillation (*i.e.* impulsive), a condition easily satisfied by ultrafast laser sources. Because the period of the oscillatory feature is hundreds of picoseconds, even the ~60 ps heat transfer process (Figure 1d), acts as an impulsive excitation for collective motions of the NPL solid, but not for breathing modes of individual particles which are expected have frequencies in the terahertz.[20,22,23] The oscillation frequency of the phonon feature of this sample (1.75 GHz) is much lower in energy than any previous observation in individual nanoparticles (5 THz-100 GHz)[18,20,23,28,45,46] and somewhat lower than previous observations in nanoparticle assemblies (5-50 GHz).[12–14]

B Thickness-Dependent Oscillations

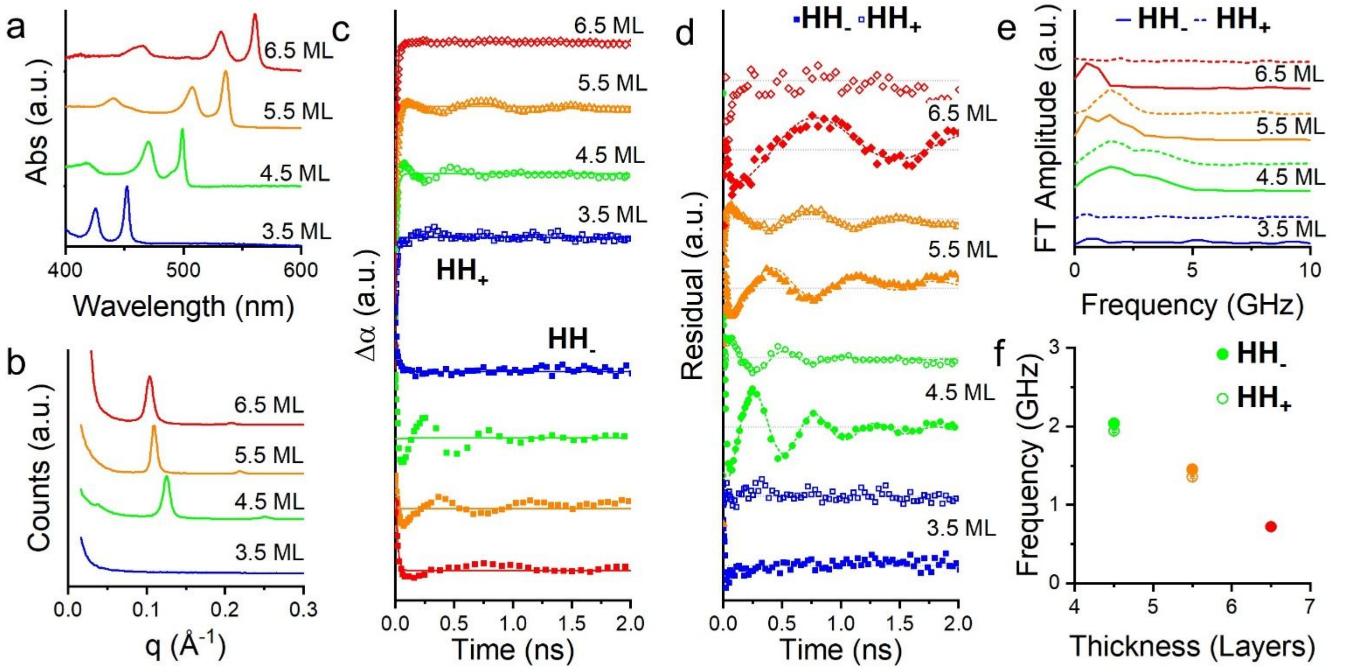

Figure 2. (a) Visible absorption spectra of solid thin films of CdSe NPLs of different thicknesses on sapphire, collected at 6 K. (b) Small-angle X-ray diffraction data collected for the same CdSe NPL samples on silica at room temperature. (c) Kinetics of IPEP measurements collected at increased and decreased transient absorption heavy-hole features for the four NPL samples. The kinetics traces are fit with exponential fits shown in solid lines. (d) Fit residuals of exponential fitting of the kinetics traces for the NPL samples of different thicknesses. The residuals are fit with exponentially damped sine waves shown in dashed lines (except for the 3.5 ML sample and 6.5 ML sample increased absorption feature). (e) Fourier transforms of the fit residuals shown in (d). (f) Sine wave frequency from fits of (d), where performed, plotted against the thickness of the NPLs. Error bars of the fits are shown, but smaller than symbols.

The oscillatory IPEP data are found for all NPL ensembles which also show interparticle ordering, but the frequency of oscillation depends upon the thickness of the NPLs. Figure 2a shows the 6 K absorption spectra of 3.5, 4.5, 5.5, and 6.5 ML CdSe NPL samples. (See Supporting Information Figure S2 for transmission electron microscopy images). The corresponding small-angle X-ray (SAXS) data for the samples is shown in Figure 2b, with a prominent reflection observed for the 4.5, 5.5, and 6.5 ML NPLs, but not in the case of the 3.5 ML NPLs. The large size of the 3.5 ML sample (39.4 nm × 21.5 nm) may impede stacking. This reflection arises from lamellar stacks of NPLs, which are widely observed in solid films and even in solutions.[34,35,47] IPEP kinetics at the heavy-hole increased and decreased absorption features for the samples at 6 K are shown in Figure 2c, with exponential fits of the rise (or decay) features shown with solid lines. Rise times of IPEP signals, which have been addressed above and in earlier work,[41,48] reflect interfacial thermal transport processes at the NPL-ligand surface.

Fitting the exponential rises of the IPEP kinetics allows the isolation, as residuals in Figure 2d, of the oscillatory component of the signal that occurs on time-scales longer than 100 ps. For the heavy-hole decreased and increased absorptions of 4.5 and 5.5 ML samples, and the transient decreased absorption of the 6.5 ML sample, the residuals show oscillatory signature persisting to 2 nanoseconds delay time, whereas the disordered 3.5 ML sample does not. (Several other 3.5 ML samples were prepared and tested without observation of acoustic phonon signatures in IPEP data.) The apparent phase of the residual signals from the HH_- and HH_+ features are shifted by $\pi/2$ with respect to each other as the first signal is negative and the second positive for the same change in band gap. In limited tests, the fluence of the IR pump beam did not change the observed frequency of oscillations (Supporting Information Figure S3). In the Fourier transform of the residual signal in Figure 2e, the oscillatory signal shifts to lower frequency for thicker NPLs. The

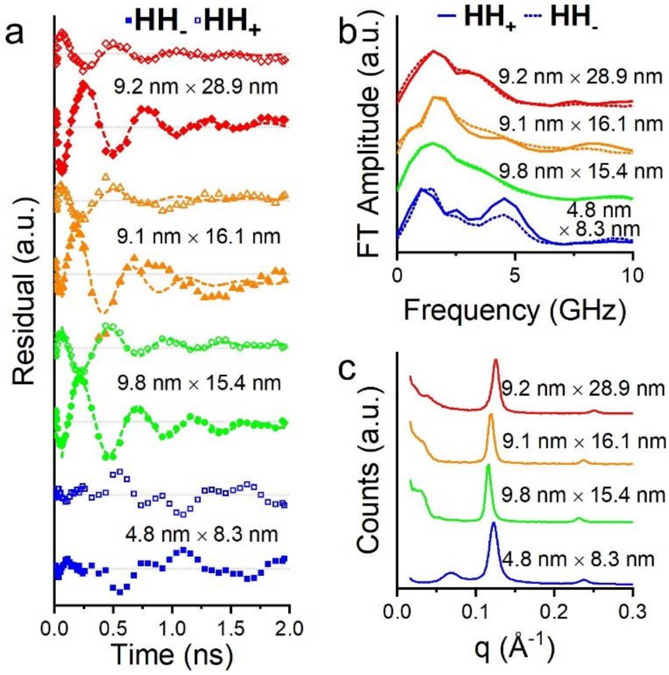

Figure 3. (a) Residuals of the monoexponential fit for 4.5 ML thick CdSe NPL samples with specified lateral dimensions. Dashed lines show a fit of the residual to an exponentially damped sine wave. The smallest NPL sample in blue is not fit to this function. Dashed gray lines indicate a residual of zero. (b) Fourier transforms of the fit residuals in (a). (c) Small-angle X-ray diffraction data collected on drop-cast films of the same NPL samples.

quality factors of the features are c. 0.5-1 for these samples. The band-width of the feature also increases as the exponential envelope of the oscillatory feature is shorter for the 4.5 ML sample than the thicker NPLs. Similarly Figure 2f shows the characteristic oscillatory frequency (from damped exponential fitting) of the acoustic phonon feature is a strong function of the NPL thickness. It was observed to vary from 0.7 GHz (1.4 ns period) for 6.5 ML NPLs to 2 GHz (500 ps period) for 4.5 ML NPLs.

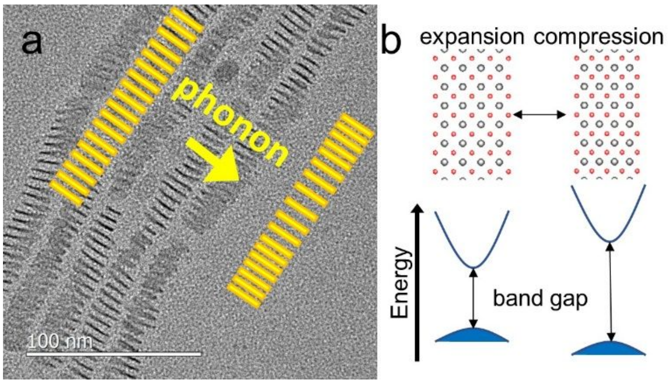

Figure 4. (a) Transmission electron microscope image of 4.5 ML CdSe NPLs forming lamellar stacks. Overlayed is a cartoon of the stack with a thermally-induced acoustic phonon. (b) Cartoon of the band gap change of 4.5 ML CdSe NPL under expansion and contraction of the lattice in the unique (short) axis.

The strong thickness dependence of the oscillatory feature was further confirmed by examining several NPLs with different lateral areas but the same 4.5 ML thickness, shown in Figure 3. Figure 3a residuals shows the residual of exponentially-fitted IPEP kinetics (see Figure S4 for raw kinetic traces of the samples) of four 4.5 ML samples at 6 K, varying in lateral area from 4.8 nm × 8.3 nm to 9.2 nm × 29 nm. Corresponding TEM images are in Supporting Information Figure S5. The Fourier transforms in Figure 3b and the results of damped sine wave fits in Figure S6 show that although the oscillatory frequency of the largest three samples are not identical, they vary over a small range (1.7 GHz to 2.1 GHz). The smallest NPL sample, however, displays a distinct temporal response which consists of more than one oscillatory signature, manifest in the splitting of the Fourier transform in Figure 3b into high and low-frequency components. The same sample is also the only one among the 4.5 ML NPLs measured to show a reflection in the SAXS measurement (Figure 3c, at 0.068 Å^{-1}) which does not arise from co-facial lamellae.

C Microscopic Origin of Oscillatory Signals

Structural data on the samples is suggestive that the origin of the oscillatory optical signal is coherent longitudinal phonons of NPL lamellae as shown in the cartoon in Figure 4a. First, referring to Figure 2, samples with strong SAXS signals associated with lamellar structure have heat-induced oscillatory transient absorption signals whereas the example without such ordering, the 3.5 ML NPLs, do not. Second, SAXS measurements of the smallest 4.5 ML sample in Figure 3c show complexity of film structure mirrored in the optical signal. Lamellar stacking of the sample with a diffraction peak at 0.123 Å^{-1}, corresponding to an NPL edge-to-edge spacing of 3.7 nm, with higher-order diffraction also observed at larger q (See Supporting Information Figure S7). But also a significant peak at 0.068 Å^{-1} corresponding to a lattice spacing of 9.2 nm, which is be attributed to the smaller 4.8 nm lateral axis of the NPLs stacking into a smectic liquid crystal. (See Supporting Information Table S1 for tabulated lattice spacings of all samples.) Third, aged films, which show substantially reduced interparticle ordering (but similar spacing) in SAXS measurements, also show much weaker oscillatory features in IPEP experiments. (See Supporting Information Figure S8.)

Such a coherent acoustic phonon in stacks of NPLs involves the subtle displacement of neighbouring plates with respect to one another and a concomitant change in band gap. These longitudinal acoustic phonons are composed of the coherent, collective expansion and contraction of the NPLs, particular in their short axis, within lamellae. Further evidence in favour of this origin is that NPLs are particularly sensitive to deformation along their unique axis. Past work has demonstrated that bulk deformation potentials are superseded in importance for CdSe NPLs by changes in the lattice along the short axis of the NPLs, due to strong quantum confinement in the shortest dimension.[49–51] Changes in the short axis length L_z from an initial value L_{z0} may be translated to a change in the band gap energy in an infinite well model with an exciton effective mass μ ($\approx 0.1m_0$)[49]

$$\Delta E = \frac{2h^2}{\mu}\left(\frac{1}{{L_z}^2} - \frac{1}{{L_{z0}}^2}\right) \tag{1}$$

Due to the quantum confined nature of the NPLs, small changes in the quantum well thickness generate perceptible changes in band gap (Figure 4b), making stacked NPLs exquisitely sensitive to deformations induced by *longitudinal* phonons. For example, the short axis deformation necessary to achieve the estimated < 200 µeV changes in band gap of the oscillatory signal are 3×10^{-3} % or smaller. Critically, this oscillatory deformation is smaller than the 1.2×10^{-2} deformation induced by thermal expansion in these experiments estimated from the temperature rise of the samples with the bulk thermal expansion coefficient of CdSe. By contrast, quantum wells are not as sensitive to biaxial strain, which adjusts the energetic spacing of light- and heavy-hole states in a manner which is not observed in these experiments.[52] It is therefore unlikely that the spectroscopic signature arises from phonons in the NPL plane. Combined with the observation that oscillatory signatures were observed only samples with lamellar order, this is supportive of an assignment of the signals to longitudinal acoustic phonons in the NPL lamellae, as shown schematically in Figure 4a.

Another possibility for the observable signal is a change in the electronic coupling of neighbouring NPLs[53] which gives rise to the oscillatory signals. For example, miniband formation has been theoretically predicted.[53] Although this phenomenon cannot be entirely ruled out, several pieces of evidence suggest that the expansion and contraction of the NPL short axis dominates. First, unambiguous thermal expansion observed in static absorption measurements nearly exactly matches the transient spectroscopic changes in IPEP measurements as shown in Figure 1c. In particular, the changes match not only at the band edge, but higher energies as well where proposed coupling of NPLs is unspecified. Furthermore, this finding applies to quantum dots and nanoplatelets in solid films and solutions, which should not display the same coupling.[41,44,48] Second, low temperature absorption measurements do not reveal a complex fine structure of the ground state lowest excitonic absorption in any NPLs (Figure 2a) and solution and solid film absorption of NPLs also show nearly identical line-shape (Figure S9) despite differences stacking. Third, the changes in band gap arising from short axis expansion are approximately 100 times greater in magnitude than those arising from miniband formation, which consequently would contribute little to the observed signal. (See Supporting Information for details of estimate.) Last, any interaction between excitons[35,42] is not relevant for these experiments in which excitation does not generate any carriers or excitons.

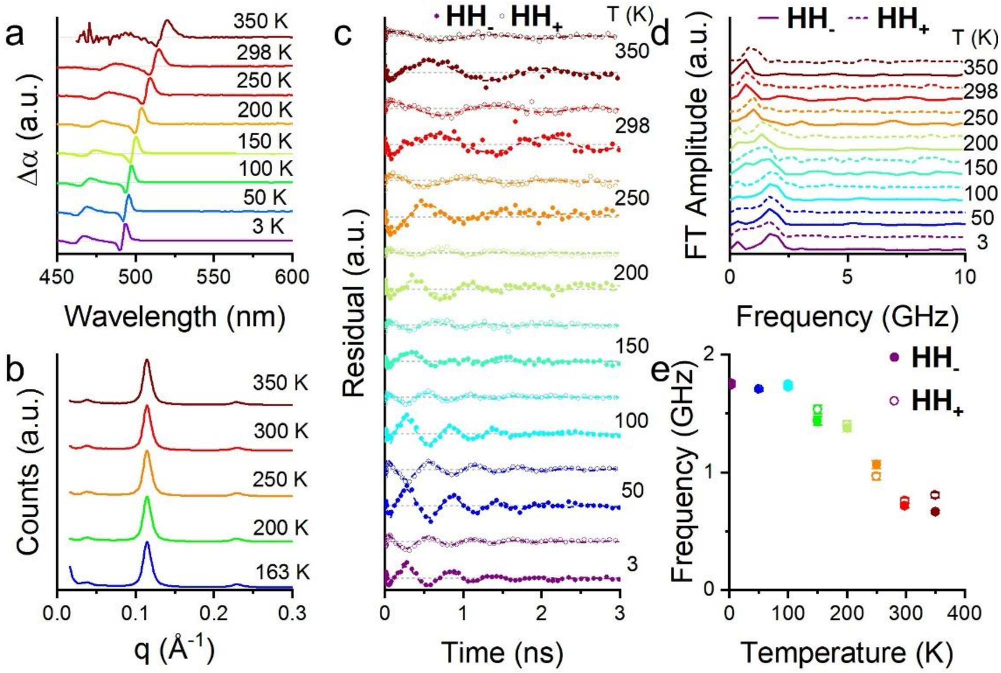

Figure 5. (a) Temperature-dependent transient absorption spectra of a 4.5 ML CdSe NPL solid sample with 3.5 µm pump and after 1 ns delay. (b) Temperature-dependent small-angle X-ray scattering of the same NPL sample. (c) Residuals of exponential fits to the increased and decreased absorption at the heavy hole features at several temperatures. Data are fitted with an exponentially damped sinusoidal function shown in dashed coloured lines. (d) Fourier transforms of residuals in (c). (e) Fitted sine wave frequencies from (c) plotted as a function of temperature. Error bars represent fitting error of residual signals.

Although the one-dimensional phonon dispersion is well-known, only one longitudinal mode is observed clearly in each sample, which precludes definition of the speed of sound. This is distinct from most picosecond acoustic experiments, including on nanocrystal superlattices,[12] but we also note that only single modes are observed in other femtosecond studies of nanocrystal superlattices.[13,14] In lieu of a phonon dispersion which may be understood from one-dimensional models, a harmonic oscillator model is employed to estimate the bonding behaviour of the organic ligands between NPLs, similar to earlier superlattices[13] and stacked gold plates.[54] The observed thickness-dependent phonon frequencies are at least qualitatively consistent with a harmonic approximation in which the oscillator angular frequency (ω) is $\omega = \sqrt{k/m}$. Previous works on spherical nanocrystals forming superlattices, which have single oscillatory frequency of 8.3 GHz, report a force constant of 1.4 ±0.2 $N\ m^{-1}$.[13] The force constants k estimated in the present work, based upon the lower frequency of phonons, fall between 0.31±0.05 N/m and 0.04±0.02 N/m, with thicker NPLs showing reduced force constants. (Errors are estimated based upon the dispersion in mass from sizing estimates.) The lower measured force constants may arise from denser ligand carpets on NPLs with less interpenetration with neighbours, which also generates larger inter-nanocrystal distances of ca. 4 nm in NPLs *versus* 3 nm observed in quasi-spherical assemblies.[13] The trend to lower k values for thicker NPL ensembles, as opposed to a fixed value of k for the ligands (Figure S10, shows that the mechanical properties of the NPL solid are not dictated solely by ligand composition. Thinner NPLs are known to show greater flexibility, forming tightly-curved scrolls, with surface curvature more like quasi-spherical nanocrystals.[55,56] Consistent with this, edge-to-edge spacings of the 5.5 ML and 6.5 ML samples are longer than those estimated for 4.5 ML samples, a factor which suppresses the acoustic phonon frequency further.

D Temperature-Dependence of Acoustic Phonons in Nanoplatelet Lamellae

As the acoustic phonon of the self-assembled NPLs offers a measure of the mechanical properties of the NPL solids, temperature-dependent measurements convey the influence of temperature on the strength of organic ligand attractive forces between NPLs. Figure 5a shows the temperature-dependent IPEP spectra for a 4.5 ML NPL ensemble (9.8 nm × 15.4 nm). These IPEP spectra closely match expected spectra from static thermal difference measurements (as in Figure 1c). From at least 163 K to 350 K, SAXS measurements showed no observable change in the lamellar spacing of the NPLs (Figure 5b; see also Supporting Information discussion and Figures S10 and S11). Under a harmonic oscillator model, this indicates that a change in the frequency of acoustic phonons (with a fixed NPL mass) is due to the stiffness of the ligands. Although the NPLs themselves (evidenced by changes in absorption) expand at higher temperatures and the ligand thermal expansion and potential glass transitions expand the specific volume[57] these changes are not discerned in the measurement (See Supporting Information for more discussion). Acoustic phonons were observed with IR excitation for this sample from 3 K up to 350 K, shown in Figure 5b, although the intensity of the oscillatory feature relative to the total signal was reduced at higher temperatures. The isolated oscillatory component in Figure 5c shows a gradual increase in the period with temperature, but also slowing of the damping effect such that at least one period is captured in the measured delay times. (Raw IPEP data can be found in Figure S13.) Fourier transforms of the residuals in Figure 5c and damped sine wave fits convey the shift from 1.75 GHz at 3 K to 0.73 GHz at 350 K. The estimated force constant k falls from 0.14±0.01 N/m at 3 K to 0.02±0.002 N/m at 350 K (Figure S10).

Although the structure of the myristic acid or oleic acid ligands on the surface of CdSe NPLs is not experimentally known, self-assembled monolayers (SAMs) offer some insights into temperature-dependent mechanical properties of long aliphatic molecules on surfaces, including disorder transitions. SAM structure depends on the surface composition and temperature, with complex phase behaviour observed in previous works.[38,39,58–60] Structural studies of SAMs show loss of diffraction at temperatures above 100 K[38] and temperature-dependent IR studies also reflect decreased chain alignment at elevated temperature.[36,37] Differential scanning calorimetry measurements of oleate ligands on spherical colloidal nanocrystals indicate a glassy transition near 200 K.[9] Similar behaviour is anticipated from the oleate layer coating the NPLs: loss of the aliphatic chain alignment of carboxylate ligands due to glassy transitions or thermal disordering weakens the inter-NPL bonds which dictate the frequency of longitudinal acoustic phonons in lamellar NPL assemblies.

Conclusion

This work demonstrates that heating excitations may be used to generate coherent acoustic phonons in stacks of semiconductor NPLs with a frequency that is largely dictated by the thickness of the NPL, which can be controlled at the atomic level. The presence of acoustic phonons of lamellar NPL stacks adds to the literature demonstrating the development of emergent or collective properties from assembled nanocrystals. The presence of coherent acoustic vibrations which subtly change the interparticle spacing of NPLs is particularly interesting in light of the strong electronic interactions of neighbouring NPLs are implicated in exceptionally-fast Förster resonance energy transfer,[35,61] charge transfer,[62] and excimer[42] or miniband formation.[53] Acoustic modulation of the inter-NPL distance offers the further possibility of extending control of optoelectronic interactions with finer spatial steps than possible with synthetic control over NPL thickness and ligand length.

Conflicts of interest

There are no conflicts to declare.

Acknowledgements

This work was performed, in part, at the Center for Nanoscale Materials, a U.S. Department of Energy Office of Science User Facility, and supported by the U.S. Department of Energy, Office of Science, under Contract No. DE-AC02-06CH11357. I. C. was supported by the University of Chicago Materials Research Science and Engineering Center, which is funded by the NSF under award number DMR-1420709. We also acknowledge support from the NSF DMREF Program under awards DMR-1629383 and DMR-1629601.

References

1 S. A. McDonald, G. Konstantatos, S. Zhang, P. W. Cyr, E. J. D. D. Klem, L. Levina and E. H. Sargent, *Nat. Mater.*, 2005, **4**, 138–142.

2 G. Konstantatos, I. Howard, A. Fischer, S. Hoogland, J. Clifford, E. Klem, L. Levina and E. H. Sargent, *Nature*, 2006, **442**, 180–183.

3 C. J. Vineis, A. Shakouri, A. Majumdar and M. G. Kanatzidis, *Adv. Mater.*, 2010, **22**, 3970–3980.

4 D. V Talapin and C. B. Murray, *Science*, 2005, **310**, 86–89.

5 V. I. Klimov, *Science*, 2000, **290**, 314–317.

6 V. L. Colvin, M. C. Schlamp and A. P. Alivisatos, *Nature*, 1994, **370**, 354–357.

7 R. Rossetti, S. Nakahara and L. E. Brus, *J. Chem. Phys.*, 1983, **79**, 1086–1088.

8 C. B. Murray, D. Norris and M. G. Bawendi, *J. Am. Chem. Soc.*, 1993, **115**, 8706–8715.

9 W. Ong, S. M. Rupich, D. V Talapin, A. J. H. Mcgaughey and J. A. Malen, *Nat. Mater.*, 2013, **12**, 410–415.

10 M. B. Zanjani and J. R. Lukes, *J. Appl. Phys.*, 2014, **115**, 143515.

11 C. B. Murray, C. R. Kagan and M. G. Bawendi, *Science*, 1995, **270**, 1335–1338.

12 C. L. Poyser, T. Czerniuk, A. Akimov, B. T. Diroll, E. A. Gaulding, A. S. Salasyuk, A. J. Kent, D. R. Yakovlev, M. Bayer and C. B. Murray, *ACS Nano*, 2016, **10**, 1163–1169.

13 I. Lisiecki, V. Halté, C. Petit, M. P. Pileni and J. Y. Bigot, *Adv. Mater.*, 2008, **20**, 4176–4179.

14 P. Ruello, A. Ayouch, G. Vaudel, T. Pezeril, N. Delorme, S. Sato, K. Kimura and V. E. Gusev, *Phys. Rev. B*, 2015, **92**, 1–6.

15 A. Courty, A. Mermet, P. A. Albouy, E. Duval and M. P. Pileni, *Nat. Mater.*, 2005, **4**, 395–398.

16 C. Thomsen, H. T. Grahn, H. J. Maris and J. Tauc, *Phys. Rev. B*, 1986, **34**, 4129–4138.

17 J. H. Hodak, A. Henglein and G. V. Hartland, *J. Chem. Phys.*, 1999, **111**, 8613–8621.

18 G. V. Hartland, *J. Chem. Phys.*, 2002, **116**, 8048–8055.

19 B. Dacosta Fernandes, M. Spuch-Calvar, H. Baida, M. Tréguer-Delapierre, J. Oberlé, P. Langot and J. Burgin, *ACS Nano*, 2013, **7**, 7630–7639.

20 D. M. Mittleman, R. W. Schoenlein, J. J. Shiang, V. L. Colvin, A. P. Alivisatos and C. V. Shank, *Phys. Rev. B*, 1994, **49**, 14435–14447.

21 T. Krauss and L. Brus, *Phys. Rev. Lett.*, 1999, **83**, 4840–4843.

22 A. V. Bragas, C. Aku-Leh, S. Costantino, A. Ingale, J. Zhao and R. Merlin, *Phys. Rev. B*, 2004, **69**, 1–11.

23 K. J. Schnitzenbaumer and G. Dukovic, *Nano Lett.*, 2018, **18**, 3667–3674.

24 E. Baldini, T. Palmieri, A. Dominguez, P. Ruello, A. Rubio and M. Chergui, *Nano Lett.*, 2018, **18**, 5007–5014.

25 L. Dworak, V. V. Matylitsky, M. Braun and J. Wachtveitl, *Phys. Rev. Lett.*, 2011, **107**, 1–5.

26 M. Pelton, Y. Wang, D. Gosztola and J. E. Sader, *J. Phys. Chem. C*, 2011, **115**, 23732–23740.

27 M. Pelton, J. E. Sader, J. Burgin, M. Liu, P. Guyot-Sionnest and D. Gosztola, *Nat. Nanotechnol.*, 2009, **4**, 492–495.

28 M. S. Kirschner, C. M. Lethiec, X. M. Lin, G. C. Schatz, L. X. Chen and R. D. Schaller, *ACS Photonics*, 2016, **3**, 758–763.

29 M. S. Kirschner, W. Ding, Y. Li, C. T. Chapman, A. Lei, X.-M. M. Lin, L. X. Chen, G. C. Schatz and R. D. Schaller, *Nano Lett.*, 2017, **18**, 442–448.

30 M. A. Van Dijk, M. Lippitz and M. Orrit, *Phys. Rev. Lett.*, 2005, **95**, 1–4.

31 T. A. Major, A. Crut, B. Gao, S. S. Lo, N. Del Fatti, F. Vallée and G. V. Hartland, *Phys. Chem. Chem. Phys.*, 2013, **15**, 4169–4176.

32 K. Yu, P. Zijlstra, J. E. Sader, Q. H. Xu and M. Orrit, *Nano Lett.*, 2013, **13**, 2710–2716.

33 P. Zijlstra, A. L. Tchebotareva, J. W. M. Chon, M. Gu and M. Orrit, *Nano Lett.*, 2008, **8**, 3493–3497.

34 S. Jana, T. N. T. Phan, C. Bouet, M. D. Tessier, P. Davidson, B. Dubertret and B. Abécassis, *Langmuir*, 2015, **31**, 10532–10539.

35 B. Guzelturk, O. Erdem, M. Olutas, Y. Kelestemur and H. V. Demir, *ACS Nano*, 2014, **8**, 12524–12533.

36 R. G. Nuzzo, E. M. Korenic and L. H. Dubois, *J. Chem. Phys.*, 1990, **93**, 767–773.

37 L. H. Dubois, B. R. Zegarski and R. G. Nuzzo, *J. Electron Spectros. Relat. Phenomena*, 1990, **54**–**55**, 1143–1152.

38 N. Camillone, C. E. D. Chidsey, G. Y. Liu and G. Scoles, *J. Chem. Phys.*, 1993, **98**, 3503–3511.

39 N. Camillone, C. E. D. Chidsey, G. Y. Liu, T. M. Putvinski and G. Scoles, *J. Chem. Phys.*, 1991, **94**, 8493–8502.

40 C. She, I. Fedin, D. S. Dolzhnikov, P. D. Dahlberg, G. S. Engel, R. D. Schaller and D. V. Talapin, *ACS Nano*, 2015, **9**, 9475–9485.

41 B. T. Diroll, P. Guo and R. D. Schaller, *Nano Lett.*, 2018, **18**, 7863–7869.

42 B. T. Diroll, W. Cho, I. Coropceanu, S. M. Harvey, A. Brumberg, N. Holtgrewe, S. A. Crooker, M. R. Wasielewski, V. B. Prakapenka, D. V. Talapin and R. D. Schaller, *Nano Lett.*, 2018, **18**, 6948–6953.

43 B. T. Diroll, I. Fedin, P. Darancet, D. V. Talapin and R. D. Schaller, *J. Am. Chem. Soc.*, 2016, **138**, 11109–11112.

44 B. T. Diroll and R. D. Schaller, *Nano Lett.*, 2019, **19**, 2322–2328.

45 J. H. Hodak, A. Henglein and G. V. Hartland, *J. Chem. Phys.*, 1999, **111**, 8613–8621.

46 T. D. Krauss and F. W. Wise, *Phys. Rev. Lett.*, 1997, **79**, 5102–5105.

47 M. D. Tessier, L. Biadala, C. Bouet, S. Ithurria, B. Abecassis and B. Dubertret, *ACS Nano*, 2013, **7**, 3332–3340.

48 B. T. Diroll and R. D. Schaller, *Nanoscale*, 2019, **11**, 8204–8209.

49 A. Antanovich, A. W. Achtstein, A. Matsukovich, A. Prudnikau, P. Bhaskar, V. Gurin, M. Molinari and M. Artemyev, *Nanoscale*, 2017, **9**, 18042–18053.

50 M. Dufour, J. Qu, C. Greboval, C. Méthivier, E. Lhuillier and S. Ithurria, *ACS Nano*, 2019, **13**, 5326–5334.

51 B. T. Diroll and R. D. Schaller, *Chem. Mater.*, 2019, **31**, 3556–3563.

52 E. P. O’Reilly, *Semicond. Sci. Technol.*, 1989, **4**, 121–137.

53 J. L. Movilla, J. Planelles and J. I. Climente, *ArXiv*, 2019, 1912.04182.

54 J. Wang, Y. Yang, N. Wang, K. Yu, G. V. Hartland and G. P. Wang, *J. Phys. Chem. A*, 2019, **123**, 10339–10346.

55 N. N. Schlenskaya, Y. Yao, T. Mano, T. Kuroda, A. V. Garshev, V. F. Kozlovskii, A. M. Gaskov, R. B. Vasiliev and K. Sakoda, *Chem. Mater.*, 2017, **29**, 579–586.

56 S. Jana, M. de Frutos, P. Davidson and B. Abécassis, *Sci. Adv.*, 2017, **3**, e1701483.

57 P. Heydemann and H. D. Guicking, *Kolloid-Zeitschrift und Zeitschrift für Polym.*, 1963, **193**, 16–25.

58 L. H. Dubois, B. R. Zegarski and R. G. Nuzzo, *J. Chem. Phys.*, 1993, **98**, 678–688.

59 H. Sellers, A. Ulman, Y. Shnidman and J. E. Eilers, *J. Am. Chem. Soc.*, 1993, **115**, 9389–9401.

60 A. Ulman, *Chem. Rev.*, 1996, **96**, 1533–1554.

61 C. E. Rowland, I. Fedin, H. Zhang, S. K. Gray, A. O. Govorov, D. V Talapin and R. D. Schaller, *Nat. Mater.*, 2015, **14**, 484–489.

62 A. Brumberg, B. T. Diroll, G. Nedelcu, M. E. Sykes, Y. Liu, S. M. Harvey, M. R. Wasielewski, M. V. Kovalenko and R. D. Schaller, *Nano Lett.*, 2018, **18**, 4771–4776.

The submitted manuscript has been created by UChicago Argonne, LLC, Operator of Argonne National Laboratory (“Argonne”). Argonne, a U.S. Department of Energy Office of Science laboratory, is operated under Contract No. DE-AC02-06CH11357. The U.S. Government retains for itself, and others acting on its behalf, a paid-up nonexclusive, irrevocable worldwide license in said article to reproduce, prepare derivative works, distribute copies to the public, and perform publicly and display publicly, by or on behalf on the Government. The Department of Energy will provide public access to these results of federally sponsored research in accordance with the DOE Public Access Plan. http://energy.gov/downloads/doe-public-access-plan.

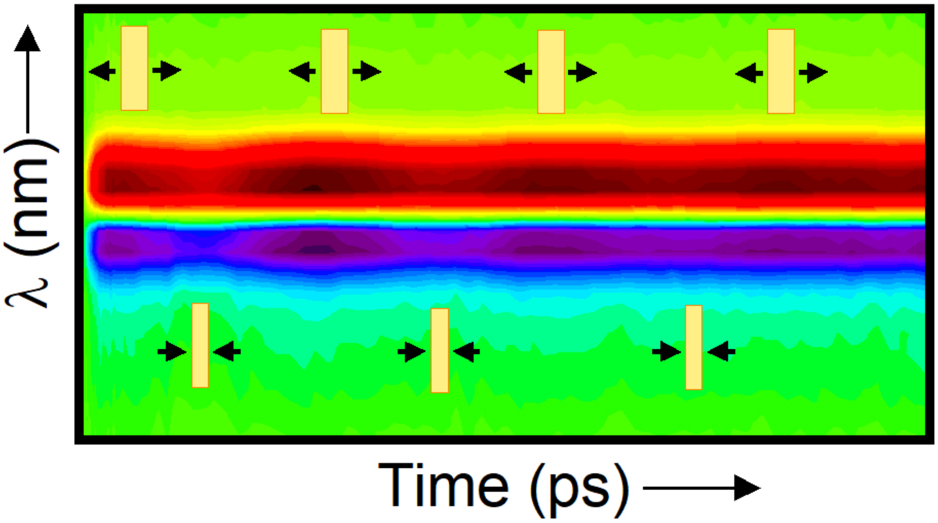
λ (nm)
Time (ps)